Title

Adult zebrafish ventricular electrical gradients as tissue mechanisms of ECG patterns under baseline vs. oxidative stress.

Journal

Cardiovascular Research, 117(8)

ISSN

1015-5007

Authors

Zhao, Yali
James, Nicholas A
Beshay, Ashraf R
et al.

Publication Date

2021-07-07

DOI

10.1093/cvr/cvaa238

Peer reviewed

ESC European Society of Cardiology

Cardiovascular Research (2021) **117**, 1891–1907
doi:10.1093/cvr/cvaa238

Adult zebrafish ventricular electrical gradients as tissue mechanisms of ECG patterns under baseline vs. oxidative stress

Yali Zhao[†,‡,¶], Nicholas A. James[‡,¶], Ashraf R. Beshay, Eileen E. Chang, Andrew Lin, Faiza Bashar, Abram Wassily, Binh Nguyen, and Thao P. Nguyen *

The Cardiovascular Research Laboratory, Division of Cardiology, Department of Medicine, David Geffen School of Medicine at UCLA, Los Angeles, CA, USA

Received 12 November 2019; revised 29 June 2020; editorial decision 23 July 2020; accepted 24 July 2020; online publish-ahead-of-print 31 July 2020

Time for primary review: 26 days

Aims In mammalian ventricles, electrical gradients establish electrical heterogeneities as essential tissue mechanisms to optimize mechanical efficiency and safeguard electrical stability. Electrical gradients shape mammalian electrocardiographic patterns; disturbance of electrical gradients is proarrhythmic. The zebrafish heart is a popular surrogate model for human cardiac electrophysiology thanks to its remarkable recapitulation of human electrocardiogram and ventricular action potential features. Yet, zebrafish ventricular electrical gradients are largely unexplored. The goal of this study is to define the zebrafish ventricular electrical gradients that shape the QRS complex and T wave patterns at baseline and under oxidative stress.

Methods and results We performed *in vivo* electrocardiography and *ex vivo* voltage-sensitive fluorescent epicardial and transmural optical mapping of adult zebrafish hearts at baseline and during acute H_2O_2 exposure. At baseline, apicobasal activation and basoapical repolarization gradients accounted for the polarity concordance between the QRS complex and T wave. During H_2O_2 exposure, differential regional impairment of activation and repolarization at the apex and base disrupted prior to baseline electrical gradients, resulting in either reversal or loss of polarity concordance between the QRS complex and T wave. KN-93, a specific calcium/calmodulin-dependent protein kinase II inhibitor (CaMKII), protected zebrafish hearts from H_2O_2 disruption of electrical gradients. The protection was complete if administered prior to oxidative stress exposure.

Conclusions Despite remarkable apparent similarities, zebrafish and human ventricular electrocardiographic patterns are mirror images supported by opposite electrical gradients. Like mammalian ventricles, zebrafish ventricles are also susceptible to H_2O_2 proarrhythmic perturbation via CaMKII activation. Our findings suggest that the adult zebrafish heart may constitute a clinically relevant model to investigate ventricular arrhythmias induced by oxidative stress. However, the fundamental ventricular activation and repolarization differences between the two species that we demonstrated in this study highlight the potential limitations when extrapolating results from zebrafish experiments to human cardiac electrophysiology, arrhythmias, and drug toxicities.

[†]Present address. Virginia Commonwealth University School of Medicine, Richmond, VA, USA.
[‡]Present address. Intervention Cardiology Department, Heart Center, University Medical Center, Ho Chi Minh City, Vietnam.
[¶]The first two authors contributed equally to the study.
*Corresponding author. Tel: +1 310 825 9465; fax: +1 310 206 5777, E-mail: tpnguyen@mednet.ucla.edu

Graphical Abstract

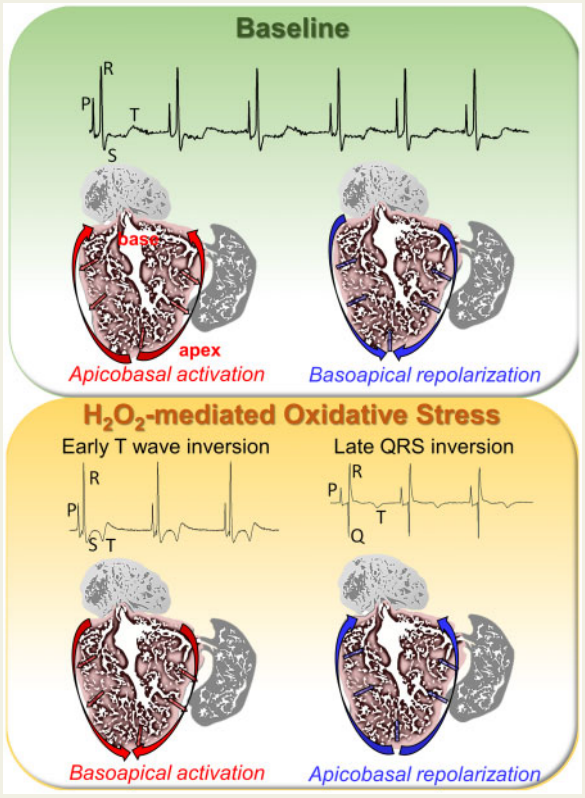

Keywords Zebrafish • Electrocardiography • Electrical heterogeneity • Electrical gradient • Oxidative stress

1. Introduction

The zebrafish (*Danio rerio*) model is a popular surrogate for human cardiac electrophysiology.[1–3] Compared with the mouse model, the heart rate, ventricular action potential, and electrocardiogram (ECG) of the zebrafish model bear closer resemblance to the human heart, suggesting that zebrafish cardiac electrophysiology is more clinically relevant.[3,4] For most drugs tested, drug responses and toxicities are also highly conserved between the zebrafish and human heart.[5,6] Therefore, zebrafish are used not only in arrhythmia mechanistic studies but also in high-throughput screening for drug-induced cardiotoxicities, particularly for ventricular repolarization toxicity as reflected by excessive QT prolongation.[7]

Despite the conservation of the ventricular action potential and ECG morphology between zebrafish and humans in health and injury,[8] the tissue electrophysiology mechanisms responsible for the inscription of the QRS complex and T wave in zebrafish remain largely unknown. In the mammalian ventricle, those tissue electrophysiological mechanisms are the electrical gradients of activation and repolarization, all of which arise from species-specific gradients of key ionic currents, Ca^{2+} handling, or gap junction proteins.[9] For example, in the healthy human ventricle, the apicobasal polarity of the repolarization gradient[9] is determined by the larger apical expression of two critical repolarizing K^+ currents—the transient outward K^+ current (I_{to}, which is absent in the zebrafish ventricle[2,10]) and the slowly activating delayed rectifier current (I_{Ks}, which is either negligible[2,10] or generated differently in the zebrafish ventricle[11]). Ventricular activation and repolarization gradients manifest in time and space as electrical heterogeneities. Because physiological electrical heterogeneities critically optimize mechanical efficiency and safeguard electrical stability,[12] the first goal of this study is to define the physiological electrical heterogeneities of the zebrafish ventricle and evaluate their conservation compared to those of the human ventricle.

Perturbation of the intrinsic electrical heterogeneities in the mammalian heart by congenital arrhythmia syndromes (such as Brugada, long, or short QT) or stress exposure (such as oxidative stress) can lead to conduction blocks and reentrant arrhythmias.[13–16] We have previously shown in intact mammalian hearts that H_2O_2-mediated oxidative stress induces triggers of arrhythmias, such as triggered activity, early and delayed afterdepolarizations (EADs, DADs), that can propagate and trigger ventricular tachycardia and fibrillation, especially when the heart is fibrotic.[17–20] However, a pathophysiological burst of localized, highly concentrated H_2O_2 is a phylogenetically conserved inflammatory response of diverse organisms, from mammals[21] to zebrafish.[22–24] Indeed, H_2O_2 signalling is so vital for zebrafish that its absence markedly impairs subsequent cardiac regeneration.[22,25] Therefore, the second goal of this study was to determine whether H_2O_2 exposure perturbs the physiological electrical heterogeneities of the healthy adult zebrafish ventricle and to assess the proarrhythmic potential of such perturbation.

2. Methods

Additional methods are available in Supplementary material online.

2.1 Ethical approval

Healthy adult (12- to 18-month-old) male and female wild-type zebrafish of the AB strain from the UCLA Zebrafish Core Facility were used for all experiments. Mean weight ranged from 500 mg to 700 mg, with females weighing more than males. Animal protocols were approved by the Institutional Animal Care and Use Committee at UCLA. The study was conducted in accordance with the US National Institutes of Health *Guide for the Care and Use of Laboratory Animals*.

2.2 Drug treatments

2.2.1 In vivo experiments

All zebrafish were immersed in 0.02–0.04% tricaine (MS-222) solution for ≤ 3 min to induce level 4 anaesthesia. At level 4 anaesthesia, zebrafish was completely immobilized and responded only to strong pressure.[26]

In the terminal *in vivo* ECG study, zebrafish received a single 100-µL intraperitoneal injection of H_2O_2 (1.7 µg or an equivalent of 2.4-3.4 mg/kg, $n = 25$) to induce oxidative stress. Control zebrafish received either no injection at all ($n = 50$) or a single 100-µL intraperitoneal injection placebo phosphate-buffered saline (PBS; $n = 10$) to assess the short-term safety of the large intraperitoneal injection volume.

In separate supplemental survival and dose–response studies (Supplementary material online, *Figures S1–S3*), besides the 1.7-µg dose, up to three additional H_2O_2 doses were used to induce oxidative stress: 0.34, 0.68, and 3.4 µg.

To assess specific inhibition of calcium/calmodulin-dependent protein kinase II (CaMKII), zebrafish received a single 50-µL intraperitoneal injection of either KN-93 (0.25 µg or an equivalent of 0.36–0.50 mg/kg; $n = 5$) or placebo KN-92 (inactive analogue, 0.28 µg or an equivalent of 0.40-0.55 mg/kg; $n = 5$).

2.2.2 Ex vivo experiments

At baseline, intact hearts were immersed in normal Tyrode's solution containing (in mM) 117 NaCl, 5.7 KCl, 4.4 $NaHCO_3$, 1.5 NaH_2PO_4, 1.8 $CaCl_2$, 1.7 $MgCl_2$, 10 Na-HEPES, 5 glucose, 5 creatine, 5 Na-pyruvic acids, and pH 7.3 adjusted with HCl. For the subsequent oxidative stress condition, H_2O_2 (100 µM) was added to the bath. Prior to or following acute H_2O_2 exposure, KN-93 (1 µM) or placebo KN-92 (1 µM) was added to assess rescue by specific CaMKII inhibition.

All *in vivo* and *ex vivo* experimental solutions were administered at room temperature (25°C). The experimental conditions were labelled in the order of drug administration if applicable: 'baseline', 'H_2O_2', 'KN93-H_2O_2', and 'KN92-H_2O_2' for pre-treatment 5 min prior to H_2O_2 exposure, or 'H_2O_2- KN93' and 'H_2O_2- KN92' for post-treatment 5 or 15 min following H_2O_2 exposure.

2.3 *In vivo* ECG

In vivo surface ECG for the healthy adult female in *Figure 1A,C,E* was selected from our pre-existing de-identified human ECG teaching library. *In vivo* surface ECG for adult zebrafish was investigated using FE136 Animal Bio Amp, PowerLab 4/35, and LabChart Pro v8 (ADInstruments) as we previously described.[27] Following complete immobilization by level 4 anaesthesia, zebrafish was transferred to a damp sponge with the ventral surface up for placement of a single bipolar ECG lead in the frontal plane. Three 29-gauge stainless steel electrodes were inserted into the zebrafish chest musculature to at most 1 mm in depth.

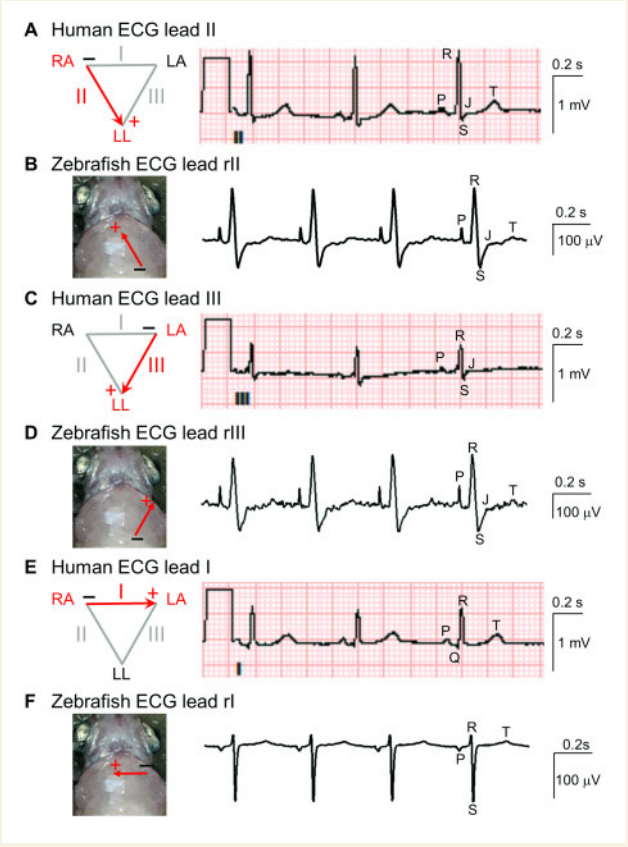

Figure 1 Comparative *in vivo* ECG lead positions and resultant ECGs from one normal adult human and one normal adult zebrafish. ECG from (*A*) the human standard bipolar limb lead II in Einthoven's triangle compared to (*B*) the zebrafish standard bipolar lead that we termed 'lead reverse (r)II' due to its opposite direction to the human lead II. Lead rII in the frontal plane is the standard lead conventionally adopted for zebrafish ECG. ECG from (*C*) the standard human lead III compared to (*D*) the zebrafish non-standard lead rIII. ECG from (*E*) the standard human lead I compared to (*F*) the zebrafish non-standard lead rI. LA, left arm; LL, left leg; RA, right arm.

All ECG leads were bipolar, in the frontal plane, and with the reference electrode positioned near the anal region. Most ECG data in this study were obtained using the standard zebrafish lead that we termed 'reverse II' (rII), with the positive electrode at the ventricular base and the negative electrode at the ventricular apex[1,8,27,28] (*Figure 1B*). Additional ECG data were obtained using non-standard leads II, reverse I (rI), and reverse III (rIII) (*Figure 1F,D*). ECG was recorded continuously: at baseline, during, and following intraperitoneal injections of KN-93 (or KN-92) and H_2O_2.

At the end of the ECG recording session in the terminal study, zebrafish was euthanized by submersion in ice water (2–4°C). In the supplemental survival studies to assess survival and ECG normalization, zebrafish was allowed to fully recover from anaesthesia as indicated by their ability to swim upright for at least 5 s.[27]

LabChart Pro v8 (ADInstruments) was used to process data off-line. The measured QT interval was normalized to the ventricular rate (or

RR interval) using the standard Bazett's formula $QTc = QT \div \sqrt{RR}$[7,27] to yield the corrected QT interval (QTc). Likewise, the measured ST interval was normalized to the ventricular rate to yield the corrected ST interval (STc). The QRS amplitude was measured as the vector sum of the positive R wave amplitude and the negative Q and S wave amplitudes. A positive QRS amplitude indicates that the R wave was dominant. A negative QRS amplitude indicates that the combined Q and S waves were dominant.

2.4 *Ex vivo* optical mapping

Following ice bath euthanasia, the zebrafish heart was rapidly removed for immediate incubation in oxygenated Tyrode's solution containing the excitation–contraction uncoupler blebbistatin (20 μM) for 45 min to suppress motion artefact during subsequent optical mapping. For the last 10 min of blebbistatin incubation, the heart was stained with the membrane voltage-sensitive fluorescent dye di-4-ANEPPS (10 μM). The stained heart was transferred to an imaging chamber containing fresh Tyrode's solution supplemented with blebbistatin (20 μM). The imaging chamber was mounted onto the stage of an upright THT macroscope (SciMedia) equipped with a high-speed complementary metal–oxide–semiconductor (CMOS) camera (MiCAM03-N256, SciMedia) with 256 × 256-pixel resolution. The field of view was 2.5 × 2.5 mm^2, yielding a spatial resolution of 9.5 μm/pixel. Fluorescence was excited with green light, delivered by a 530-nm LEX2-LZ4-G light-emitting diode (SciMedia) through a 531/40-nm excitation filter (Semrock). The excitation light was split by a 560-nm dichroic mirror (Semrock) and filtered by a 600-nm long-pass filter (Hoya). The emitted fluorescence was collected by a 5× objective lens (Leica) and projected by a 135-mm projection lens (Samyang). *Ex vivo* optical action potentials were recorded at 1 ms/frame. Epicardial mapping was performed on the frontal plane of intact hearts. Transmural mapping was performed on the coronal plane of wedge preparations from partially resected hearts with intact sinoatrial and atrioventricular conduction.

2.5 Data analysis and definitions

Optical signals were analysed using specialized software (BVAna, Brainvision). Noise was reduced by cubic filtering (3 × 3 pixels). Ventricular activation duration is the time required for activation of the entire ventricle, measured as the temporal difference between activation of the first and last pixel in the ventricle. Action potential duration at 90% of repolarization (APD_{90}) is the time between the largest slope during the entire upstroke $(dV_m/dt)_{max}$ and 90% of repolarization from peak amplitude. Ventricular ΔAPD_{90} is the temporal difference between the shortest and the longest ventricular APD_{90}. Repolarization time at 90% of repolarization (RT_{90}) is the sum of activation time and APD_{90}. Ventricular repolarization duration is the temporal difference ΔRT_{90} between the shortest and the longest ventricular RT_{90}. Ventricular electrical gradient is a key index that relates the electrical propagation time to the ventricular length, measured as the maximal apicobasal dimension. Hence, ventricular gradients of activation, APD, and repolarization were calculated by adjusting ventricular activation duration, ΔAPD, and repolarization duration, respectively, for ventricular length.

2.6 Statistical analysis

Statistical analysis was performed using GraphPad Prism8. Data were expressed as mean ± standard deviation (SD), [95% CI], and *P*-value. The 95% confidence interval [95% CI] was estimated using the bootstrap-resampling method with 10 000 replications.[29] Due to the non-normality of the H_2O_2 data distribution as assessed by normal quantile plots and Shapiro–Wilk test, non-parametric statistical tests were applied for all experimental conditions.[30] Statistical significance of differences was evaluated using one-way ANOVA with Tukey's *post hoc* analysis for comparison of experimental groups and Wilcoxon signed-rank test or chi-square test for comparison of experimental conditions to which the same ventricle was exposed. $P < 0.05$ was the minimal standard for statistical significance.

3. Results

Additional figures are available in Supplementary material online.

3.1 Tissue mechanism of the normal QRS complex

The configuration and duration of the QRS complex reflect the spread of ventricular activation. Our goal was to define the tissue mechanism responsible for the normal QRS of healthy adult zebrafish. First, we performed *in vivo* ECG. Based on the direction of the mean QRS vector, we predicted the underlying ventricular activation gradient. To verify our prediction, we performed *ex vivo* voltage-sensitive fluorescent optical mapping to determine the contributions of the epicardial and transmural ventricular activation gradients.

For our *in vivo* ECG investigations (*Table 1*), we used the zebrafish standard bipolar lead 'reverse II' (rII),[27] unless otherwise specified. Compared to the positive electrode of the human standard bipolar lead II at +60° relative to the heart (*Figure 1A*), the positive electrode of the standard zebrafish lead rII is at -120° relative to the heart (*Figure 1B*).

The normal zebrafish QRS in lead rII and the normal human QRS in lead II are similar morphology and positive polarity (*Figure 2A*). By definition, the Q and S deflections are negative whereas the R deflection is positive. The polarity of the largest deflection (R vs. Q + S) determines the net polarity of the QRS complex. Analogous to the small human Q wave in lead II, which is present in only 48% of normal adults,[31] the zebrafish Q wave in lead rII under baseline stress-free condition was also the smallest wave of the QRS complex and visible in only 71% of normal wild-type zebrafish in this study. Like the human S wave in lead II, the zebrafish S wave in lead rII at baseline was smaller than the R wave in the same lead (*Figure 1A,B*). Analogous to the dominant human R wave in lead II, the zebrafish R wave in lead rII was invariably dominant at baseline. Because the zebrafish QRS in lead rII was positive at baseline (*Table 1*, *Figures 1B and 2A*), the QRS vector must point from the apex (rII negative electrode) to base (rII positive electrode). Thus, we predicted that the tissue mechanism of the normal adult zebrafish QRS complex is a ventricular activation gradient with apicobasal polarity.

Although sex difference in QRS duration was reported for humans,[32] none reached statistical significance in this zebrafish study. The mean baseline QRS duration was 33 ± 9 ms for $n = 14$ males and 35 ± 8 ms for $n = 6$ females, $P > 0.05$. Because the zebrafish J point often defies accurate identification,[8,27] we followed the common practice in the field to slightly underestimate the zebrafish QRS duration by measuring from the start of the Q wave (or R wave if the Q wave is absent) to the readily identifiable peak of the S wave,[27] rather than to the elusive J point (*Table 1*). Using this method to evaluate QRS duration, the underestimate was roughly 15 ms at baseline in our study. For example, in the healthy 12-month-old female zebrafish in *Figure 1B*, the QRS duration was 35 ms to the S peak or 50 ms to the J point. In either estimate, this zebrafish QRS was shorter than the 90-ms QRS of the healthy 27-year-old woman in

Table 1 ***In vivo*** **ECG lead rII of the normal adult zebrafish ventricle**

ECG parameters	Baseline ($n = 20$)	H_2O_2 ($n = 15$)	KN93-H_2O_2 ($n = 5$)
QRS amplitude (μV)	104 ± 60 [77,131]	-7 ± 28 [-22,7]***	95 ± 47 [36,153]^{NS,*}
QRS polarity (% of *n*)			
Positive (upright)	**100**%	40%	**100**%
Negative (inverted)	–	**60**%	–
T wave amplitude (μV)	15 ± 12 [9,20]	-7 ± 7 [11,2]****	13 ± 13 [-3,29]^{NS,**}
T wave polarity (% of *n*)			
Positive (upright)	**90**%	–	**100**%
Negative (inverted)	5%	**87**%	–
Flat (isoelectric)	5%	13%	–
QRS duration (ms)	33 ± 9 [30,38]	70 ± 24 [56,84]****	37 ± 8 [26,46]^{NS,**}
STc duration (ms)	358 ± 59 [323,386]	433 ± 61 [379,448]**	368 ± 43 [346,389]^{NS,*}
QTc duration (ms)	401 ± 88 [361,441]	517 ± 67 [477,558]***	461 ± 53 [395,527]^{NS,*}

The QRS amplitude is the vector sum of the positive R wave amplitude and the negative Q and S wave amplitudes. Dominant polarities are highlighted in bold. Data are expressed as mean ± SD [95% CI]. *P*-value symbols are shown in black for comparison of either stress group (H_2O_2 or KN93-H_2O_2) with the baseline group and in red for comparison of the KN93-H_2O_2 group with the H_2O_2 group.
$^{*}P < 0.05$,
$^{**}P < 0.01$,
$^{***}P < 0.001$,
$^{****}P < 0.0001$,
$^{NS}P > 0.05$; one-way ANOVA with Tukey's *post hoc* analysis.
QTc, corrected QT interval; STc, corrected ST interval.

Figure 1A. Because QRS reflects ventricular activation, this finding indicates that ventricular activation in zebrafish must be more rapid than in humans.

To supplement data from lead rII configuration, we constructed an axial reference system analogous to Einthoven's triangle, but in reverse orientations. In our zebrafish 'reverse Einthoven's triangle', the orientations of the three leads rII, rIII, and rI relative to the heart are -120°, -60°, and 180°, respectively (*Figure 1B,D,F*). Given that current zebrafish ECG data acquisition systems are limited by a single-lead configuration, we constructed the reverse Einthoven's triangle sequentially (*Figure 1B,D,F*), rather than simultaneously as done in humans (*Figure 1A,C,E*). We repositioned one electrode at a time to record from leads rIII and rI ($n = 5$) after recording from the standard lead rII. The normal QRS was positive in lead rIII ($n = 5$; *Figure 1D*) like in lead rII, once again reaffirming the prediction that normal zebrafish ventricular activation spread from apex to base. However, the normal QRS in lead rI was negative ($n = 5$) (*Figure 1F*), suggesting that normal ventricular activation at the base spread from right to left of the frontal plane.

To verify the predicted tissue mechanism of the normal QRS complex, epicardial optical mapping was performed on the frontal plane of intact hearts ($n = 21$). At baseline, epicardial ventricular activation spread rapidly within 13 ms from apex to base (*Table 2*, *Figure 3B*). Thus, the epicardial ventricular activation gradient (*Figure 4A*, *Table 2*) accounted for the baseline positive QRS polarity in leads rII (*Figures 1 and 2B*) and rIII (*Figure 1*).

3.2 Tissue mechanism of the normal ST and QT interval

The configuration and duration of the ST segment and T wave reflect the spread of ventricular repolarization. Our goal was to define the tissue mechanism responsible for the normal ST segment and T wave of healthy adult zebrafish.

Our *in vivo* ECG investigation of healthy adult zebrafish revealed that at baseline, the T wave in leads rII ($n = 20$) and rIII ($n = 5$) was invariably smaller than the R wave in the same respective leads (*Figure 2A,B*, *Table 1*). Importantly, both the QRS complex and the T wave in leads rII ($n = 18/20$; *Figure 2A,B*) and rIII ($n = 5/5$; *Figure 1D*) were positive. Therefore, healthy adult zebrafish displayed 'positive concordance' between QRS and T wave in leads rII and rIII under baseline condition as healthy adult human hearts do in leads II and III. The positive polarity of the T wave in leads rII and rIII suggested that normal ventricular repolarization spread from base to apex. Additionally, the positive T wave concordance implies that the main direction of ventricular repolarization is opposite to that of the preceding ventricular activation. Based on the finding of T wave concordance in leads rII and rIII at baseline, we predicted an inverse relationship between activation time and repolarization time. Because ventricular activation time was longest at the base and shortest at the apex, we predicted that ventricular APD_{90} and repolarization time would be, inversely, shortest at the base and longest at the apex.

In *Figure 1*, the QTc duration of 409 ms in the healthy 18-month-old female zebrafish was comparable to the QTc duration of 448 ms in the healthy 27-year-old woman. Therefore, comparing to the human counterparts, while the normal zebrafish QRS duration (*Figure 2C*) was invariably shorter as noted above, the normal zebrafish QTc duration (*Figure 2C*) fell within the normal human range, suggesting that the normal zebrafish STc duration (*Figure 2C*) must be at least as long as in humans. We predicted that unlike normal zebrafish ventricular activation, which was ultra-rapid as shown in Section 3.1, normal zebrafish ventricular APD_{90} and repolarization time were as slow as seen in humans.

To verify the predicted tissue mechanism of the normal ST interval, epicardial optical mapping was performed on the frontal plane of intact hearts ($n = 21$). As predicted from the ventricular ECG patterns, epicardial mapping revealed that at baseline, the base was the first to repolarize

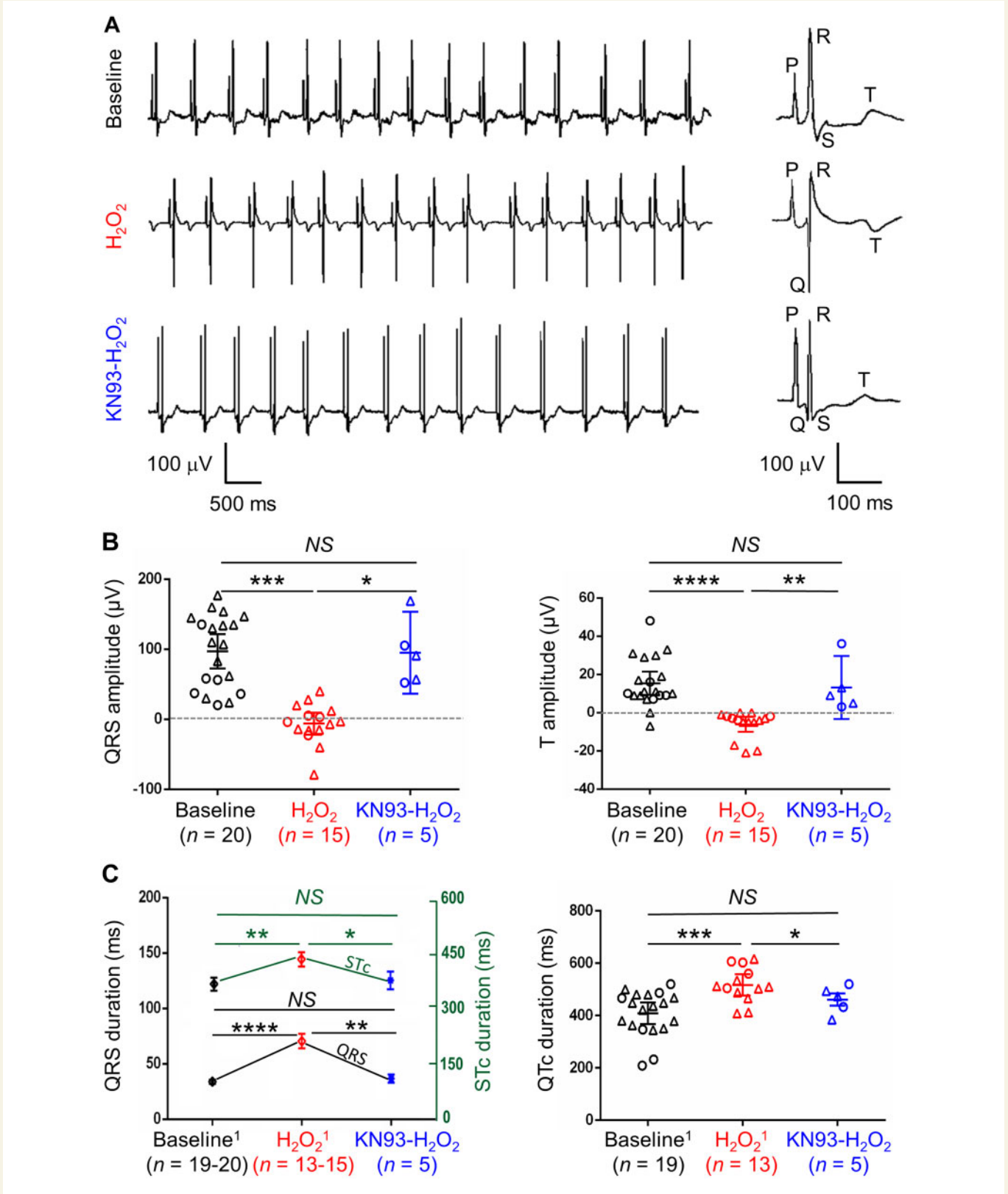

Figure 2 Comparative *in vivo* ventricular ECG patterns under baseline and oxidative stress conditions. (*A*) Representative ECG tracings and higher magnification of a single cardiac cycle from healthy adult zebrafish under three different experimental conditions. (*Top row*) At baseline of this fish, the QRS and T wave concordance was positive because both the QRS complex and T wave were positive. (*Middle row*) In the same fish as shown in the top row, H_2O_2 inverted the QRS and T wave concordance to negative (by inverting both QRS and T) and prolonged the QT interval (by prolonging both QRS and the ST interval). (*Bottom row*) In another healthy fish with similar baseline ECG as shown in the top row, pre-treatment with KN-93 protected the ventricular ECG patterns from perturbations by subsequent H_2O_2 exposure. (*B,C*) ECG was acquired from 20 live fish at baseline then again following intraperitoneal H_2O_2 administration, but only 5 of these 20 fish received KN-93 pre-treatment prior to H_2O_2 administration. (*B*) Amplitudes and polarities of the QRS complex

Table 2 Epicardial electrical gradients of the normal adult zebrafish ventricle

Epicardial gradients	Baseline ($n = 21$)	H_2O_2 ($n = 15$)		KN93-H_2O_2 ($n = 6$)
Ventricular activation gradient				
AT_{base}[a] (ms)	13 ± 2 [12,14]	0****	24 ± 6 [19,30]****	14 ± 2 [13,16]^{NS}
AT_{apex}[a] (ms)	0	24 ± 6 [17,30]****	0^{NS}	0^{NS}
AT apex vs. base[§]	$P < 0.0001$	$P < 0.0001$	$P < 0.0001$	$P < 0.0005$
Polarity (% of *n*)				
Apicobasal	**100**%		47%	**100**%
Basoapical	0%	**53**%		0%
Duration[b] (ms)	13 ± 2 [12,14]	24 ± 7 [20,28]***		14 ± 2 [13,16]^{NS,*}
Magnitude[c] (ms/mm)	9 ± 1 [8,10]	17 ± 5 [15,20]***		11 ± 1 [10,12]^{NS,*}
Ventricular APD_{90} gradient				
$APD_{90,\ base}$ (ms)	235 ± 29 [219,251]	319 ± 40 [274,326]****	287 ± 43 [238,347]***	232 ± 32 [199,265]^{NS}
$APD_{90,\ apex}$ (ms)	263 ± 23 [244,272]	298 ± 45 [275,312]**	309 ± 39 [279,339]**	261 ± 33 [227,295]^{NS}
APD_{90} apex vs. base[§]	$P < 0.0001$	$P < 0.0005$	$P < 0.005$	$P < 0.0005$
Polarity (% of *n*)				
Apicobasal	0%	**73**%		0%
Basoapical	**100**%		27%	**100**%
$\lvert\Delta APD_{90}\rvert$ (ms)	22 ± 12 [21,39]	32 ± 17 [13,45]*		23 ± 11 [16,30]^{NS,*}
Magnitude[c] (ms/mm)	16 ± 8 [9,26]	24 ± 15 [9,35]*		17 ± 5 [10,24]^{NS,*}
Ventricular repolarization gradient				
$RT_{90,\ base}$ (ms)	244 ± 25 [234,263]	337 ± 35 [313,362]****	281 ± 31 [238,324]***	247 ± 23 [238,271]^{NS}
$RT_{90,\ apex}$ (ms)	261 ± 26 [243,275]	303 ± 38 [276,335]***	301 ± 34 [256,337]**	264 ± 24 [234,291]^{NS}
RT_{90} apex vs. base[§]	$P < 0.005$	$P < 0.0005$	$P < 0.05$	$P < 0.05$
Polarity (% of *n*)				
Apicobasal	0%	**60**%		0%
Basoapical	**100**%		40%	**100**%
Duration[b] (ms)	12 ± 6 [9,28]	21 ± 14 [12, 32]*		13 ± 4 [12,21]^{NS,*}
Magnitude[c] (ms/mm)	9 ± 3 [5,16]	18 ± 10 [9,25]*		10 ± 2 [6,15]^{NS,*}

[a]The zero reference activation time (AT) is the AT of the ventricular region first to activate.
[b]Activation or repolarization duration is the absolute difference between basal and apical activation or repolarization times.
[c]Gradient magnitude is the electrical duration normalized to ventricular length.
Data are expressed as mean ± SD [95% CI]. *P*-value symbols are shown in black for comparison of either stress group (H_2O_2 or KN93-H_2O_2) with the baseline group and in red for comparison of the KN93-H_2O_2 group with the H_2O_2 group.
$^{*}P < 0.05$.
$^{**}P < 0.01$.
$^{***}P < 0.001$.
$^{****}P < 0.0001$,
$^{NS}P > 0.05$; one-way ANOVA with Tukey's post hoc analysis.
[§]*P*-values are listed for comparison of apex with base in the same ventricle under the same test condition.
APD_{90} (or RT_{90}), action potential duration (or repolarization time) at 90% of repolarization.

and the apex the last. The epicardial gradient of ventricular APD_{90} was oriented in the basoapical direction, with APD_{90} being shortest at the base and longest at the apex ($n = 15$; *Figure 3A,C*, *Table 2*). Because repolarization time at 90% of repolarization (RT_{90}) is the sum of the rather brief activation time and the much longer APD_{90}, the epicardial basoapical polarity of the repolarization gradient reflected primarily that of the APD_{90} gradient (*Figure 3B–D*, *Table 2*). In other words, when comparing all three epicardial electrical gradients, the APD_{90} gradient correlated negatively with the moment of activation and positively with the moment of repolarization. Thus, the epicardial ventricular repolarization gradient (*Figure 4B,C*, *Table 2*) accounted for the baseline positive T wave concordance in leads rII and rIII.

3.3 Acute perturbations of ventricular electrical gradients by H_2O_2

Exposure of the mammalian ventricle to injury, disease, or oxidative stress can perturb baseline physiologic electrical gradients.[15,16,33] For example, perturbation of the ventricular activation and repolarization gradients in myocardial infarction results in pathologic Q wave

Figure 2 Continued
and T wave. The QRS amplitude was measured as the vector sum of the positive R wave amplitude and the negative Q and S wave amplitudes. (*C*) Durations of the QRS complex and the corrected STc and QTc intervals. When T wave was flat (as seen in 1 fish at baseline and 2 fish after H_2O_2 exposure), ST_C and QT_C could not be assessed. Symbols: Δ, male; O, female; bar and whiskers, mean ± SD. $^{*}P < 0.05$, $^{**}P < 0.01$, $^{***}P < 0.001$, $^{****}P < 0.0001$, $^{NS}P > 0.05$; one-way ANOVA with Tukey's *post hoc* analysis.

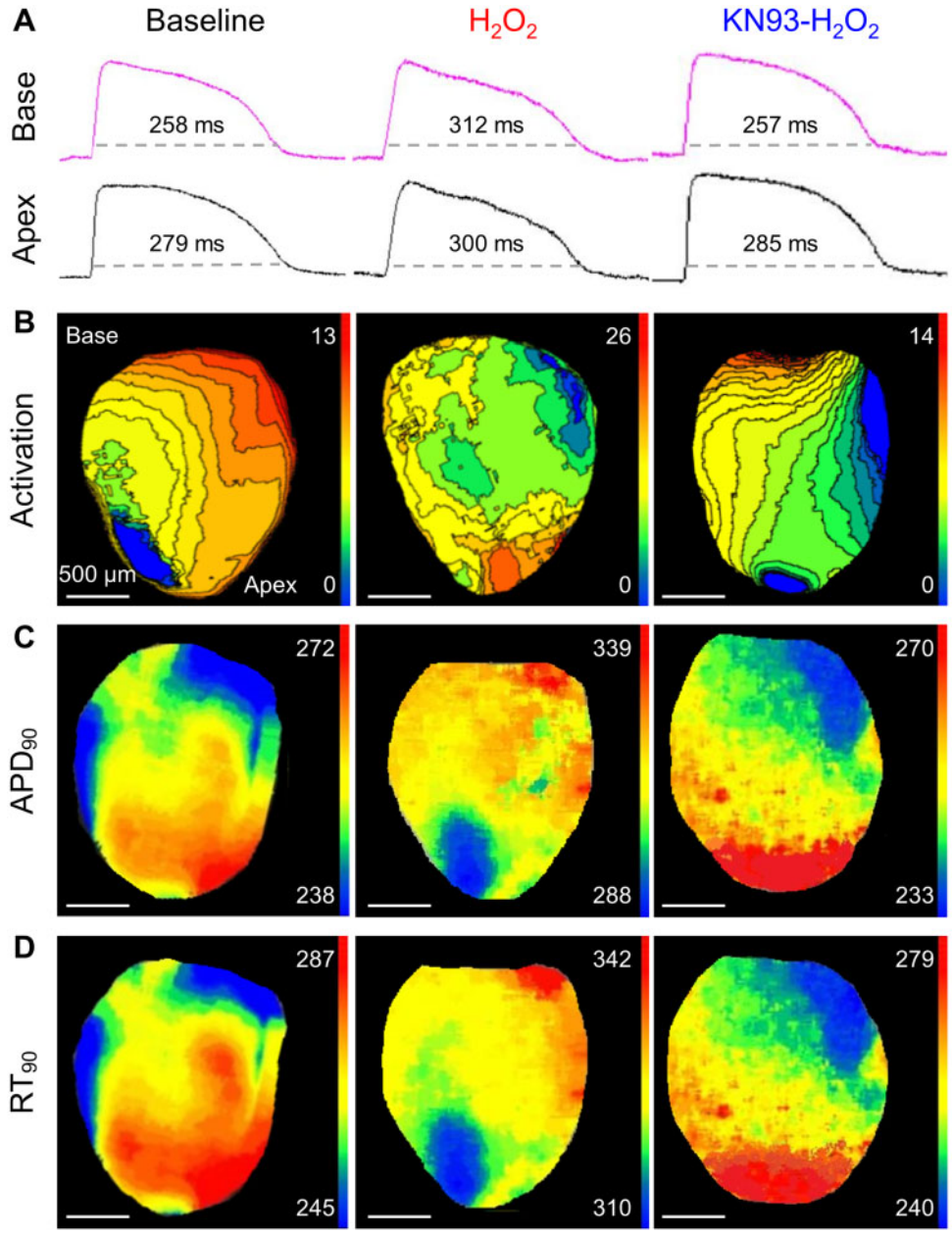

Figure 3 Comparative ventricular optical action potentials and electrical heterogeneities under baseline and oxidative stress conditions. (*A*) Representative optical ventricular action potentials from two *ex vivo* hearts (the same heart for baseline and H_2O_2 and another heart for KN93-H_2O_2) showed that slurring of the upstroke and prolongation of the plateau by H_2O_2 exposure was prevented by pre-treatment with KN-93. (*B*) Representative ventricular activation maps from one heart showed that H_2O_2 doubled the activation duration and reversed the direction of the activation spread by impairing activation at the apex more severely than at the base. Pre-treatment with KN-93 of another heart protected the ventricle from activation impairment by subsequent H_2O_2 exposure. Isochrones are 1-ms for baseline and KN93-H_2O_2 maps, 2-ms for H_2O_2 map. (*C*) Representative APD_{90} maps and (*D*) repolarization time RT_{90} maps from one heart showed that H_2O_2 prolonged repolarization and reversed the direction of the repolarization spread by impairing repolarization at the base more severely than at the apex. Pre-treatment with KN-93 of another heart protected the ventricle from repolarization impairment by subsequent H_2O_2 exposure. Scale: 500 µm.

development and T wave inversion,[33] respectively. Our goal was to determine whether acute exposure of the normal zebrafish ventricle to H_2O_2-mediated oxidative stress perturbed baseline electrical gradients, causing pathologic ECG abnormalities.

Following *in vivo* ECG investigation in lead rII at baseline, intraperitoneal H_2O_2 was administered ($n = 15$). Comparison with baseline revealed that H_2O_2 significantly prolonged the QRS duration and inverted the QRS complex, prolonged the ST interval and inverted or flattened the T wave (*Table 1*, *Figure 2*). These new ventricular ECG abnormalities indicated that H_2O_2 impaired both activation and repolarization of the zebrafish ventricle. In 27% of fish ($n = 4/15$), H_2O_2 inverted both the QRS complex and the T wave, thereby reversing the polarity of

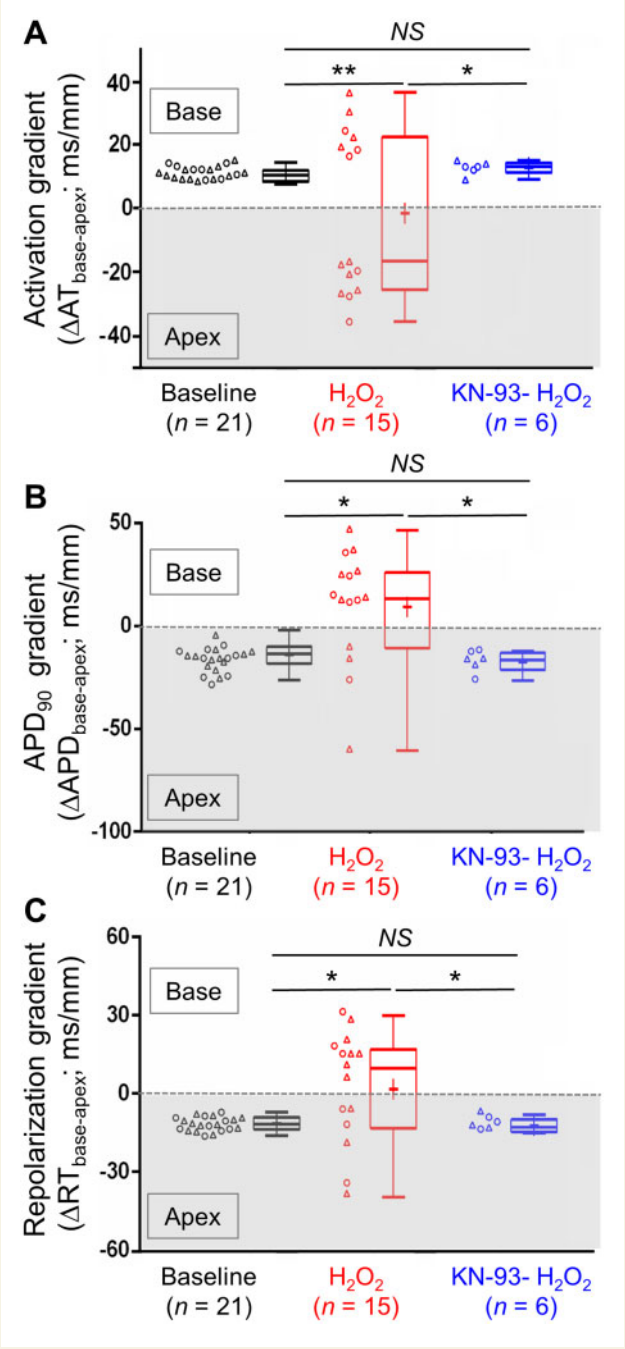

Figure 4 Comparative ventricular electrical gradients under baseline and oxidative stress conditions. (*A–C*) Optical mapping was performed on 21 intact hearts at baseline then again following H_2O_2 exposure, but only 6 of these 21 hearts received KN-93 pre-treatment prior to H_2O_2 exposure. H_2O_2 reversed all three electrical gradients of the ventricular epicardium. Pre-treatment with KN-93 protected the gradients from H_2O_2 perturbations. Symbols: box plots with mean (+), median, first, and third quartiles (box), minimum and maximum (whiskers), together with individual data; Δ, male; O, female. $^{*}P < 0.05$, $^{**}P < 0.005$, $^{NS}P > 0.05$; one-way ANOVA with Tukey's *post hoc* analysis. RT, repolarization time.

the T wave concordance from positive to negative (Supplementary material online, *Figure S4*). In another 60% of fish ($n = 9/15$), H_2O_2 inverted only the T wave and diminished the R wave amplitude without inverting the QRS complex, thereby causing new T wave discordance (or loss of baseline T wave concordance). We predicted that the mechanisms underlying these H_2O_2-induced QRS and T wave abnormalities were acute perturbations of the ventricular electrical gradients.

Interestingly, the dose-dependent H_2O_2-induced perturbations of ventricular ECG patterns followed a specific fixed sequence (Supplementary material online, *Figure S2*). T wave and QRS inversions occurred only at intraperitoneal H_2O_2 doses $\geq 0.68\,\mu g$. However, T wave inversion preceded QRS inversion, indicating that the reversal of the ventricular repolarization gradient preceded the reversal of the ventricular activation gradient. We compare this sequence of ventricular ECG perturbation to the sequence of normalization in Section 3.7 (Supplementary material online, *Figure S3*).

Following *ex vivo* epicardial optical mapping under baseline condition, hearts were exposed to H_2O_2 ($n = 15$) and voltage-mapped again after at least 10 min of H_2O_2 exposure. Comparison of epicardial optical action potentials within the same ventricular region under baseline vs. stress condition revealed that H_2O_2 impaired both activation and repolarization as evidenced by prolongation of activation time, APD, and repolarization time (*Figure 4*, *Table 2*). Importantly, the impairment severities were different for different ventricular regions. When H_2O_2 impaired activation more severely at the apex than the base, the base became first to activate and the apex last. Conversely, when H_2O_2 impaired repolarization and prolonged APD more severely at the base than the apex, the base completed repolarization after the apex and basal APD_{90} became more prolonged than apical APD_{90}. These divergent, region-dependent impairments explained how H_2O_2 inverted the epicardial gradients of activation in 53% ventricles (*Figures 3A,B* and *4A*, *Table 2*), of APD in 73% ventricles, and of repolarization in 60% ventricles (*Figures 3C,D* and *4B,C*, *Table 2*), consistent with ECG predictions. H_2O_2 perturbations of the ventricular activation gradient prolonged the activation duration and amplified the activation gradient magnitude (*Table 2*). In contrast, H_2O_2 perturbations of the ventricular APD and repolarization gradients did not amplify the gradient magnitudes (*Table 2*). The reason is that such perturbations were so heterogeneous even in the same ventricular region that the resultant increases in local APD and repolarization dispersion within the same ventricular region paradoxically led to decreases in global dispersion.

3.4 Sex differences

Human sex differences in certain ECG parameters, such as T wave amplitude, QRS, and QTc duration, have been documented.[32,34,35] In this study, we did not detect any significant sex differences in ECG or ventricular action potential characteristics of adult male and female wild-type zebrafish of the AB strain under baseline or oxidative stress condition, likely because our sample size was not large enough to permit detection of small differences, if any, recorded from a single limb lead.

3.5 Proarrhythmic consequences of H_2O_2 for the normal zebrafish heart

H_2O_2 disrupted *in vivo* sinus node activity, causing sinus arrhythmias in 93% of fish ($n = 14/15$) and fluctuations of the sinus rate that ranged from acceleration ($n = 7/15$), deceleration ($n = 13/15$), to transient complete arrest ($n = 9/15$) (*Figure 5B–D*, *Table 3*). To visualize and quantify how H_2O_2 perturbed the dynamics of beat-to-beat heart rate variability (HRV), we constructed Poincaré plots[36–38] (Supplementary material online, *Figure S5*). After fitting an ellipse to the Poincaré plot shape, we computed the Poincaré indexes SD1, SD2, and SD1/SD2 ratio. SD1, the

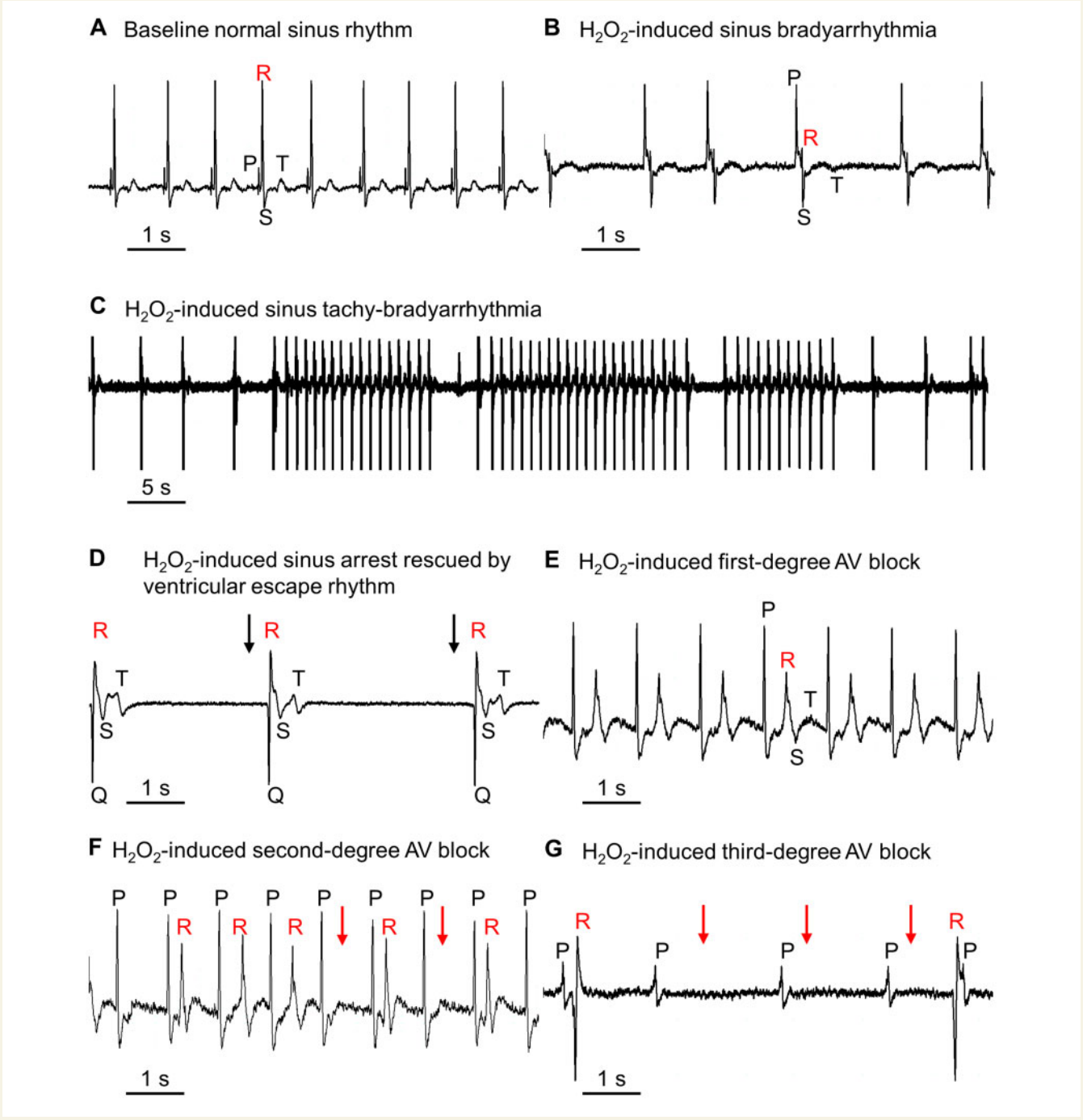

Figure 5 Acute *in vivo* proarrhythmic perturbations of the healthy zebrafish heart by H_2O_2 exposure. (*A–G*) Each panel displays ECG from one live fish (*A*) at normal baseline or (*B–G*) following intraperitoneal H_2O_2 administration. H_2O_2 induced proarrhythmic perturbations (*B–D*) at the sinus node, (*E*) the atrium, (*F, G*) the atrioventricular (AV) node and ventricular conduction system. Although no cardiac structures were immune from H_2O_2 proarrhythmic perturbations, full-blown tachyarrhythmias did not emerge in these healthy non-fibrotic zebrafish ventricles ($n = 0/15$). Symbols: (↓) missing R wave; (↓) missing P wave.

ellipse half-width, measures the dispersion of data perpendicular to the line of identity and reflects the standard deviation of the successive differences of the RR intervals. SD2, the ellipse half-length, measures the spread of data along the line of identity and reflects the standard deviation of the RR intervals. The SD1/SD2 ratio represents the randomness in the HRV time series. We found that at baseline, the Poincaré plot pattern was a tight cluster, indicating that there was very little dispersion in the HRV time series of healthy zebrafish under level 4 anaesthesia (SD1/SD2 was ~1), similar to the behaviour of a denervated heart in transplant patients. However, following H_2O_2 intraperitoneal injection, the Poincaré plot pattern became complex with greater SD1 and disproportionate rise in SD2, resulting in a halving of SD1/SD2 ratio. This

Table 3 Proarrhythmic consequences of H_2O_2 for the normal adult zebrafish heart

***In vivo* proarrhythmia**	**Baseline ($n = 20$)**	**H_2O_2 ($n = 15$)**	**KN93-H_2O_2 ($n = 5$)**
Heart rate (b.p.m.)	103 ± 15 [96,110]	62 ± 46 [37,88]***	109 ± 21 [82,134]^{NS}
Heart rhythm (% of n)	**Normal sinus rhythm (100%)**	**Sinus bradyarrhythmia (47%)***	**Normal sinus rhythm (100%)^{NS}**
		Sinus tachy-bradyarrhythmia (40%)	
		Sinus tachyarrhythmia (7%)	
		Normal sinus rhythm (7%)	
Sinus arrest[a] (% of *n*)	0%	60% ($n = 9$)	0%
Max sinus pause (ms)	N/A	7249 ms	N/A
Escape rhythm			
Junctional	N/A	11% (1/9 fish)	N/A
Ventricular	N/A	22% (2/9 fish)	N/A
Absent	N/A	67% (6/9 fish)	N/A
AV conduction[b] (% of n)			
Normal	100%	20% ($n = 3$)	100%
Abnormal	0%	80% ($n = 12$)	0%
1st-degree AV block	N/A	100% (12/12 fish)	N/A
2nd-degree AV block	N/A	50% (6/12 fish)	N/A
3rd-degree AV block	N/A	8% (1/12 fish)	N/A
Ventricular standstill	N/A	17% (2/12 fish)	N/A
***Ex vivo* proarrhythmia**	**Baseline ($n = 21$)**	**H_2O_2 ($n = 15$)**	**KN93-H_2O_2 ($n = 6$)**
Cycle length (ms)	563 ± 48 [525,623]	1333 ± 227 [1211,1728]***	584 ± 64 [538,631]^{NS}
Heart rhythm (% of n)	**Normal sinus rhythm (100%)**	**Sinus bradyarrhythmia (80%)*** **	**Normal sinus rhythm (100%)^{NS}**
		Sinus tachy-bradyarrhythmia (14%)	
		Sinus tachycardia (7%)	
Sinus arrest[a] (% of *n*)	0%	53% ($n = 8$)	0%
Max sinus pause (ms)	N/A	7496 ms	N/A
Escape rhythm			
Junctional	N/A	13% (1/8 hearts)	N/A
Ventricular	N/A	13% (1/8 hearts)	N/A
Absent	N/A	75% (6/8 hearts)	N/A
AV conduction[b] (% of *n*)			
Normal	100%	7% ($n = 1$)	100%
Abnormal	0%	93% ($n = 14$)	0%
1st-degree AV block	N/A	100% (14/14 hearts)	N/A
2nd-degree AV block	N/A	14% (2/14 hearts)	N/A
3rd-degree AV block	N/A	7% (1/14 hearts)	N/A
Ventricular standstill	N/A	7% (1/14 hearts)	N/A
Arrhythmia triggers (% of *n*)			
Triggered activity	0%	A (20%) V (0%)	0%
DAD	0%	A (0%) V (0%)	0%
EAD	0%	A (0%) V (0%)	0%

[a]Sinus arrest is defined in this study as the transient absence of *in vivo* P waves or *ex vivo* atrial action potentials lasting ≥1.5 s.
[b]H_2O_2 could cause multiple types of atrioventricular (AV) block in the same hearts.
The most predominant heart rhythms are highlighted in bold. Numerical data are expressed as mean ± SD [95% CI] . Statistical analysis to compare either stress condition (H_2O_2 or KN93-H_2O_2) with baseline condition to which the same ventricles were exposed: Wilcoxon signed-rank test for heart rate comparison; two-tailed chi-square for dominant heart rhythm comparison.
*$P < 0.01$,
***$P < 0.0001$,
$^{NS}P > 0.05$.
A, atrium; AV, atrioventricular; DAD/EAD, delayed/early afterdepolarization; V, ventricle.

finding indicated the emergence of chaos caused by H_2O_2-mediated increased dispersion in the HRV time series. Importantly, at baseline the RR intervals were short and converged at the lower-left corner of the Poincaré plot, indicating rapid heart rate. In contrast, under H_2O_2 condition, the dispersion of the RR intervals over the entire plot indicated that H_2O_2 intermittently slowed the heart into the bradycardic range, known to promote the emergence of EADs and ventricular tachyarrhythmias in humans and other mammals.[18]

H_2O_2 also impaired cardiac conduction at all tissue levels. Impaired atrial conduction was evidenced by H_2O_2-induced first-degree AV block

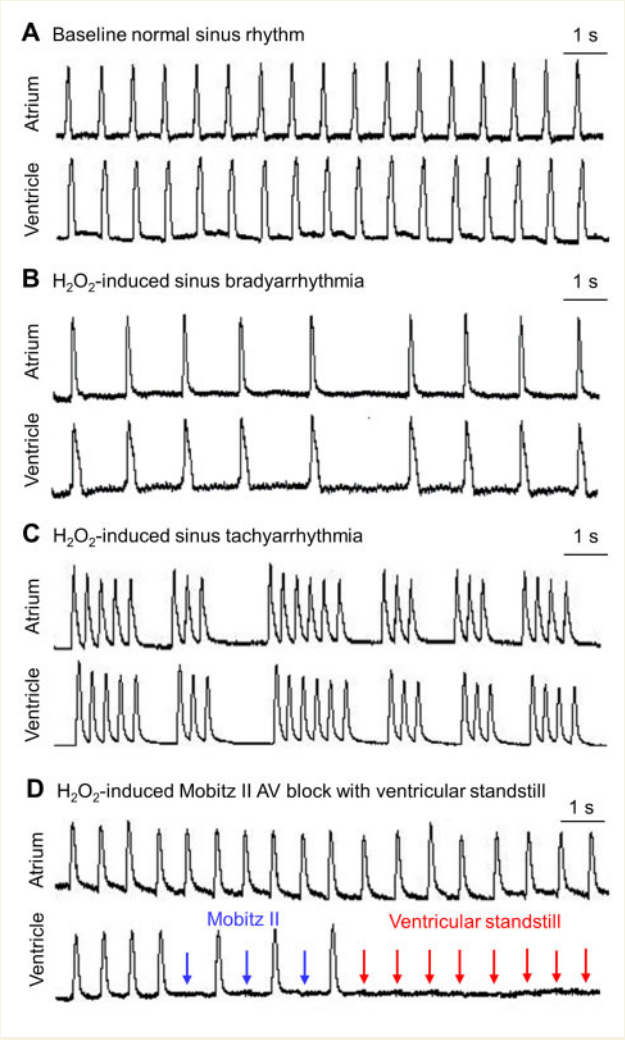

Figure 6 Acute *ex vivo* proarrhythmic perturbations of the healthy zebrafish heart by H_2O_2 exposure. (*A–D*) Each panel displays optical action potentials from one intact heart (*A*) at normal baseline or (*B–D*) following H_2O_2 exposure. H_2O_2 disrupted *ex vivo* sinus node rhythm and rate, (*B*) slowing the pacemaker rate or (*C*) speeding it up with bursts of triggered activity. (*D*) H_2O_2 dampened conduction in the atrioventricular (AV) node and ventricular conduction system. Triggers of arrhythmias or full-blown tachyarrhythmias did not emerge in these healthy non-fibrotic ventricles ($n = 0/15$). Symbol: (↓) missing ventricular action potential.

(i.e. PR prolongation) in 80% of fish ($n = 12/15$; *Figure 5E*, *Table 3*). Impaired atrioventricular (AV) node conduction was evidenced by second-degree block Mobitz type I ($n = 3/15$), Mobitz type II ($n = 3/15$), and rare third-degree block ($n = 2/15$) (*Figure 5F,G*, *Table 3*). Because conduction velocity was inversely related to activation gradient, impaired ventricular conduction was evidenced by impaired activation, which reflected as significant prolongation of QRS ($n = 15/15$). Additionally, although H_2O_2 prolonged QTc ($n = 13/15$ with identifiable T wave) and caused the loss of positive T wave concordance ($n = 15/15$) (*Table 1*), H_2O_2 did not elicit in vivo reentrant ventricular tachyarrhythmias at intraperitoneal H_2O_2 doses of ≤1.7 μg.

Epicardial voltage mapping of *ex vivo* intact hearts ($n = 15$; *Figure 6*) agreed with *in vivo* ECG findings. Because H_2O_2 prolonged ventricular activation duration nearly two-fold (13 ms at baseline vs. 24 ms under H_2O_2 condition; *Table 2*), H_2O_2 slowed ventricular conduction by nearly two-fold. Importantly, like H_2O_2-induced activation impairment, H_2O_2-induced conduction delay was region-dependent and in 53% ventricles more severe at the apex. The heterogeneity of repolarization impairment by H_2O_2 was even more apparent. Even within the same ventricular region, the repolarization behaviour during H_2O_2 exposure appeared chaotic and dynamic neighbouring macroscopic 'islands' emerged at different stages of repolarization (Supplementary material online, *Figure S6*). However, H_2O_2 at concentrations of ≤100 μM did not induce focal triggers of arrhythmias or propagating ventricular tachyarrhythmias in healthy, non-fibrotic zebrafish ventricular substrates. Instead, the recurrent bursts of triggered activity observed in the ventricle resulted from H_2O_2 modulation of the sinus node electrical activity, which was then conducted 1:1 through the AV node to the ventricle (*Figure 6C*).

3.6 Protection of ventricular gradients from H_2O_2 perturbations by CaMKII inhibition

Using immunofluorescence staining, we found that H_2O_2 activated CaMKII in a concentration-dependent fashion (Supplementary material online, *Figure S7*). We also found that *in vivo* and *ex vivo* KN-93-mediated blockade of CaMKII activation 5 min prior to H_2O_2 exposure effectively protected the zebrafish heart from subsequent H_2O_2 proarrhythmic perturbations. ECG obtained following H_2O_2 administration revealed that KN-93 pre-treatment protected all zebrafish from significant QRS widening, QT prolongation, and loss of positive concordance of the T wave with QRS ($n = 5/5$; *Figure 2*, *Table 1*). Consistent with ECG findings, optical mapping following H_2O_2 exposure revealed that KN-93 pre-treatment protected all ventricles from significant impairment of activation and repolarization and from reversal of electrical gradients. KN-93 pre-treatment also preserved baseline ventricular gradients of activation, APD, and repolarization for all hearts ($n = 6/6$; *Figure 4*, *Table 2*). However, pre-treatment with the inactive analogue KN-92 also failed to protect the zebrafish ventricles from proarrhythmic perturbations during subsequent *in vivo* ($n = 5$) or *ex vivo* ($n = 6$) H_2O_2 exposure.

In contrast to KN-93 effective protection in pre-H_2O_2 treatment, KN-93 rescue in post-H_2O_2 treatment was much less effective. The longer the H_2O_2 exposure prior to KN-93 treatment, the lower the success rate of KN-93 rescue. For example, KN-93 administered at 5 min post-H_2O_2 ($n = 13$) could restore baseline ventricular activation and APD gradients in only 50% of hearts ($n = 6/12$ and 5/10, respectively) and baseline repolarization gradient in only 27% of hearts ($n = 3/11$) (Supplementary material online, *Figure S8*). In comparison, KN-93 administered at 15 min post-H_2O_2 ($n = 5$) failed to restore baseline ventricular electrical gradients in any zebrafish ($n = 0/5$).

3.7 Transmural ventricular electrical gradients under baseline and H_2O_2 condition

Transmural mapping was performed on the coronal plane of wedge preparations from partially resected hearts with intact sinus and atrioventricular conduction ($n = 9$). Transmural ventricular activation spread rapidly from endocardium to epicardium whereas transmural ventricular repolarization spread from epicardium to endocardium (Supplementary material online, *Figure S9*). Therefore, the transmural ventricular activation gradient could not account for the baseline positive QRS polarity in leads rII (*Figures 1 and 2B*) and rIII (*Figure 1*). Nor could the transmural

ventricular repolarization gradient account for the baseline positive T wave concordance in leads rII and rIII. Importantly, transmural mapping following H_2O_2 exposure ($n = 6$) revealed that over this short transmural distance of ≤100 μm, H_2O_2 did not reverse the endo-to-epicardial activation gradient or the epi-to-endocardial repolarization gradient (Supplementary material online, *Figure S9*).

3.8 Survival and normalization following H_2O_2 exposure

In the terminal *in vivo* ECG study, all control and H_2O_2-treated healthy adult zebrafish tolerated ECG recording ($n = 85$) and intraperitoneal injection ($n = 45$) well with no complications. Zebrafish also tolerated treatments with tricaine ($n = 85$), PBS ($n = 10$), H_2O_2 ($n = 25$), KN-93 ($n = 5$), and KN-92 ($n = 5$) well. At the end of the ECG recording session, all zebrafish were alive and required euthanasia, except for the 2 out of 25 H_2O_2-treated zebrafish. These two H_2O_2-treated zebrafish, which did not receive KN-93 pre-treatment, developed ventricular standstill (*Table 3*) following complete heart block and expired after ECG recording was complete at ≥10 min post-H_2O_2 induction. ECG from control zebrafish that received PBS intraperitoneal injection did not differ from prior to injection ($n = 10$) or from control zebrafish receiving no injection ($n = 50$).

Additionally, two survival studies were performed. The dose-survival study aimed to assess over a longer time window of up to 48 h post-injection the safety of large intraperitoneal injection volume of 100 μL and the dose-dependence of H_2O_2 toxicity. We measured the survival rates of four groups of zebrafish, all anaesthetized to level 4 with tricaine, at three endpoints: Day 0 post-injection (dpi 0) after full recovery from anaesthesia, dpi 1, and dpi 2 (Supplementary material online, *Figure S1*). The four groups ($n = 10$ per group) consisted of zebrafish treated with (i) tricaine only, (ii) tricaine + PBS, (iii) tricaine + 1.7 μg H_2O_2, and (iv) tricaine + 3.4 μg H_2O_2. The dose-survival curves confirmed that fish of 12–18 months of age tolerated well the large injection volume and the oxidative stress mediated by 1.7 μg of H_2O_2 (the only dose used in the terminal study).

The second survival study ($n = 5$) aimed to determine whether the H_2O_2-perturbed ventricular ECG patterns normalized at dpi 2 following H_2O_2 metabolism and to dissect the sequence of normalization (Supplementary material online, *Figure S3*). We found that at dpi 2 following intraperitoneal injection of 1.7 μg H_2O_2, normalization of the negative QRS complex completed in all fish ($n = 5/5$), but normalization of the negative T completed in only 3 of 5 fish and only started in the remaining 2 fish. These findings had three implications. First, the healthy adult zebrafish heart could produce enough antioxidants within 48 h to neutralize the exogenous 1.7 μg of H_2O_2 dose. Second, the ventricular activation gradient was restored before the ventricular repolarization gradient. Lastly, because the T wave was first to invert and last to normalize, the sequence of normalization (Supplementary material online, *Figure S2*) was opposite the sequence of perturbation (Supplementary material online, *Figure S3*). In other words, zebrafish ventricular repolarization was more susceptible to H_2O_2 perturbation than zebrafish ventricular activation.

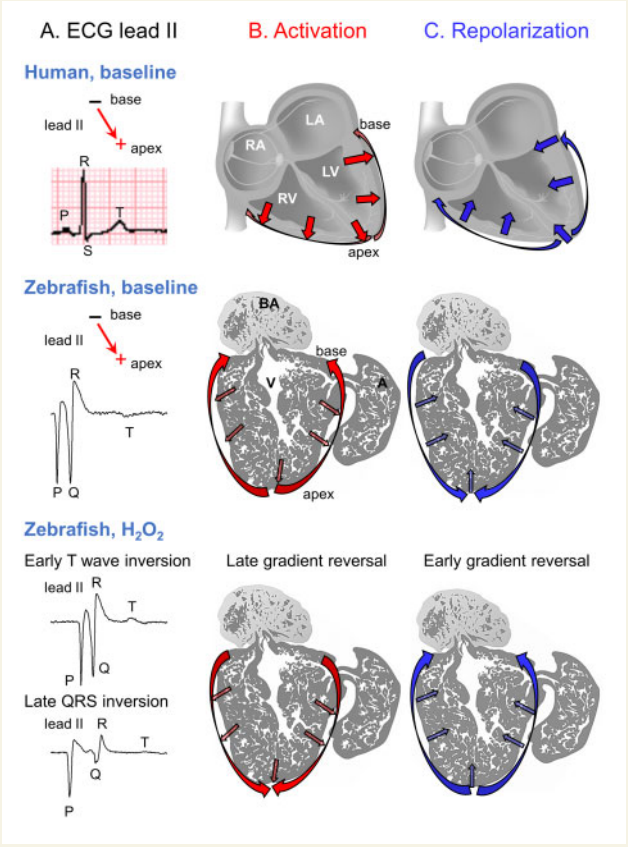

Figure 7 Divergent tissue mechanisms for human and zebrafish ventricular ECG patterns. (*A*) Under baseline condition, human and zebrafish ventricular ECG patterns in lead II are mirror images across the isoelectric baseline. The QRS and T wave concordance in lead II is positive in humans and negative in zebrafish. In practice, however, for the zebrafish to display human-like positive QRS and T wave concordance, lead rII (with reverse polarity to lead II) is conventionally used. (*B*) While the baseline epicardial and transmural activation gradients of the human and zebrafish ventricle superficially share similar polarities, their mechanistic contributions to generate mirror-image QRS complex are different. In the human ventricle, the net spread of activation towards lead II (+) electrode at the apex to generate a positive QRS deflection (R > S) is due to the transmural gradient alone. In contrast, in the zebrafish ventricle, the net spread of activation away from lead II (+) electrode at the apex to generate a negative QRS deflection (R < Q) is due to the epicardial gradient alone. H_2O_2 may reverse this epicardial gradient, causing QRS inversion from negative to positive (R > Q). (*C*) Likewise, the baseline human and zebrafish ventricular repolarization gradients contribute differently to generate mirror-image T wave. In the human ventricle, the net spread of repolarization away from lead II (+) electrode at the apex to generate a positive T wave may be due to either or both the transmural gradient and the epicardial gradient. In contrast, in the zebrafish ventricle, the net spread of repolarization towards lead II (+) electrode at the apex to generate a negative T wave is due to the epicardial gradient alone. H_2O_2 may reverse this epicardial gradient, causing T wave inversion from negative to positive. A, atrium; BA, bulbus arteriosus; RA/LA, right/left atrium; RV/LV, right/left ventricle; V, ventricle.

4. Discussion

4.1 Electrical heterogeneities as tissue mechanisms of ventricular ECG patterns

Despite the popular use of the zebrafish heart as a surrogate model for human cardiac electrophysiology and cardiomyopathies, our understanding of zebrafish cardiac electrical heterogeneity has been limited. The substantial homology between the zebrafish and human cardiac response to a broad range of drugs[7,39,40] provides the impetus for the

application of zebrafish as a high-throughput screening tool for potential drug-induced cardiotoxicities in humans, such as QT prolongation. Indeed, the adult zebrafish and human hearts share remarkable parallels in morphology and duration of several ECG features. In health, both species display concordance of the R and T waves. In myocardial ischaemia, both species may display ST-segment depression and T wave inversion, QRS widening and QT prolongation.[8] Yet, whether the underlying ventricular repolarization dynamics of these two species are actually similar, as the similarities in their ECG features seem to suggest, was unknown. In this study, we performed *in vivo* ECG and *ex vivo* optical mapping to define the ventricular gradients of activation, APD and repolarization in healthy adult zebrafish.

We found that in healthy adult zebrafish ventricles, normal spontaneous activation proceeded rapidly from apex to base (consistent with Sedmera *et al.*)[41] and from endocardium to epicardium (*Figure 7B*). Therefore, both the zebrafish epicardial and transmural gradients of ventricular activation appeared to resemble those in healthy adult humans (*Figure 7B*). However, this resemblance was only superficial because ventricular activation gradients with similar polarity must give rise to QRS waveforms with similar, not opposite, polarity if the QRS waveforms are obtained from the same lead. Although the zebrafish and human QRS waveforms obtained from the standard zebrafish lead rII and standard human lead II were both positive, these two leads have opposite polarities and are mirror image of each other. Indeed, the zebrafish QRS waveform that we obtained from in the equivalent of human lead II was a negative, mirror image of the positive human QRS in the same lead (*Figure 7A*). Therefore, we conclude that the net ventricular activation gradient of zebrafish and humans point in opposite directions. In the human heart, only the transmural gradient of ventricular activation accounts for the positive QRS waveform in lead II because the endo-to-epi transmural wave of depolarization moves towards lead II positive electrode at the apex. The human epicardial gradient of ventricular activation makes negligible contribution because the apicobasal epicardial wave of depolarization moves away from, instead of towards, lead II positive electrode (*Figure 7A,B*). In contrast, in the zebrafish heart, the apicobasal epicardial gradient of ventricular activation fully accounted for the positive QRS waveform in lead rII because only the epicardial, but not the transmural, wave of depolarization, moved towards lead rII positive electrode at the base (*Figure 7A,B*).

In addition, we found that in healthy zebrafish ventricles, normal spontaneous ventricular repolarization proceeded in reverse directions to ventricular activation, from base to apex and from epicardium to endocardium (*Figure 7C*). While the zebrafish transmural gradients of ventricular APD and repolarization superficially resembled those in normal adult humans, the zebrafish epicardial gradients were opposite to those in normal adult humans. In the human heart, both the epicardial and transmural gradients of repolarization can account for the positive T wave in lead II as they both point away from lead II positive electrode at the apex. In contrast, in the zebrafish heart, the basoapical gradient of ventricular repolarization fully accounted for the positive T wave in lead rII because only the epicardial, but not the transmural, wave of repolarization, moved away from lead rII positive electrode at the base (*Figure 7*). Therefore, we conclude that the net ventricular repolarization gradient of zebrafish and humans proceed in opposite directions, just like their opposite net ventricular activation gradient.

QRS and T wave concordance requires that repolarization must proceed in a reverse direction to activation. While both human and zebrafish ventricles display positive QRS and T wave concordance at a healthy baseline, the two species have divergent underlying tissue mechanisms. Whereas human ventricles rely primarily on transmural electrical gradients, zebrafish ventricles rely on epicardial gradients instead. This mechanistic difference may stem from structural differences. The adult human ventricular myocardium is thick and compact. In contrast, the adult zebrafish ventricular myocardium is partitioned into a trabeculated inner layer and a thin outer compact layer entirely covered by the epicardium, known to be critical for cardiac repair and regeneration.[42]

4.2 The arrhythmogenic risk of H_2O_2 for adult zebrafish hearts

In adult zebrafish hearts following injury, inflammatory H_2O_2 signalling is required to drive structural remodelling and myocardial regeneration.[25] The role of H_2O_2 is so vital that attempts to scavenge H_2O_2 or prevent H_2O_2 generation markedly impair cardiac regeneration.[25] However, in mammalian hearts, H_2O_2 is arrhythmogenic. We previously showed at the isolated mammalian myocyte level that H_2O_2 prolongs APD and the action potential plateau through oxidative CaMKII activation-dependent induction of repolarization failure or EADs.[18–20,43] We also showed at the intact mammalian heart level that H_2O_2-induced triggers of arrhythmias, such as EAD- and DAD-mediated triggered activity, could propagate and mediate ventricular tachycardia and fibrillation in the fibrotic aged or diseased heart, but not in the normal healthy heart.[17,18] In the zebrafish heart, it is unclear whether the long-term benefit for regeneration mediated by H_2O_2 comes at the cost of a short-term risk of life-threatening arrhythmias. To our knowledge, this study is the first to define the proarrhythmic potential of healthy uninjured adult zebrafish hearts by acute H_2O_2-mediated oxidative stress and to draw correlates with H_2O_2 electrical perturbation of healthy uninjured mammalian hearts.

First, H_2O_2 impaired both activation and repolarization processes of the healthy adult zebrafish ventricle. By impairing ventricular activation, H_2O_2 widened QRS. By impairing repolarization, H_2O_2 prolonged APD, thereby prolonging the ST and QT intervals (*Figure 2C*). Second, H_2O_2 reversed the polarity of the epicardial gradients of ventricular activation, APD, and repolarization, thereby inverting the QRS complex and/or T wave and perturbing their positive concordance. Third, the ventricular electrical perturbation by H_2O_2 was spatially heterogeneous. However, this spatial heterogeneity followed fixed regional specificities (base vs. apex) overall, despite appearing chaotic within the same ventricular region (base or apex). Specifically, H_2O_2-induced perturbation of activation followed a fixed predilection for the apex whereas perturbation of repolarization followed a fixed predilection for the base. This spatial heterogeneity exhibited a similar epicardial pattern among different H_2O_2-treated hearts (Supplementary material online, *Figure S10*) and was quasi-stable on a consecutive beat-to-beat basis within the same heart (Supplementary material online, *Figure S11*). However, the detailed patterns of activation (or repolarization) within the same region (apex or base) were non-uniform and varied across different H_2O_2-treated hearts (Supplementary material online, *Figure S10*) and across non-consecutive beats within the same heart (Supplementary material online, *Figure S11*). Consequently, H_2O_2 amplified the intrinsic apicobasal dispersion of APD and repolarization, which could predispose the ventricle to the development of potentially lethal reentrant arrhythmias.[44]

4.3 CaMKII activation as a mediator for H_2O_2 arrhythmogenesis: an old mechanistic relationship in a new heart model?

In rabbit and rat isolated ventricular isolated myocytes and intact fibrotic hearts, we and others have demonstrated that CaMKII activation is a critical molecular determinant for H_2O_2 induction of ventricular EADs, triggered activity, tachycardia, fibrillation, and torsades de pointes.[17,18,43,45–47] Activation of CaMKII signalling facilitates the enhancement of I_{to},[48] late I_{Na},[45,49] $I_{Ca,L}$, and late $I_{Ca,L}$.[50] Discontinuing H_2O_2 exposure or inhibiting CaMKII activation can suppress H_2O_2-induced emergence of EADs and ventricular tachycardia or fibrillation.[43] To the best of our knowledge, this study was the first to demonstrate that activation of CaMKII signalling is also responsible for H_2O_2 proarrhythmic modulation of adult zebrafish ventricles. We showed that specific inhibition of CaMKII activation using KN-93 effectively protected baseline electrical heterogeneities from subsequent H_2O_2 perturbations, both *in vivo* and *ex vivo*.

4.4 Utility of the adult zebrafish heart model for arrhythmogenesis studies

This study demonstrated that in normal adult zebrafish hearts (Supplementary material online, *Figure S12*), H_2O_2 caused spatially non-uniform conduction slowing and action potential prolongation sufficiently to reverse the ventricular electrical gradients, but these perturbations did not sufficiently reduce the protective source-sink mismatch of the normal non-fibrotic heart to induce spontaneous ventricular tachyarrhythmias. These findings are compatible with our prior observations of normal non-fibrotic adult mammalian hearts treated with H_2O_2.[17] We and others have previously demonstrated that H_2O_2 impairs ventricular repolarization of the normal mammalian heart[17] and readily promotes spontaneous triggers of arrhythmias (such as EADs, DADs, and triggered activity) in single myocytes isolated from normal mammalian hearts.[18,19,43] However, these proarrhythmic perturbations by H_2O_2 alone were insufficient to enable local arrhythmia triggers that emerged in a few myocytes to propagate to the remaining healthy ventricular tissue to initiate spontaneous ventricular tachycardia and fibrillation, unless the ventricle was remodelled by myocardial fibrosis due to injury, disease, or aging.[17,51,52]

The clinical utility of the adult zebrafish heart model for studies of arrhythmogenesis is further enhanced by a clinically relevant anatomical and electrophysiological feature of the zebrafish ventricle, the His-Purkinje system. Sedmera *et al.* argued that two PSA-NCAM-positive main trabecular bands that span the entire adult zebrafish ventricle from the atrioventricular junction to the apex represent a functional equivalent of the His-Purkinje system because their ablation resulted in complete heart block.[41] Here, our findings that *in vivo* and *ex vivo* H_2O_2-treated zebrafish hearts developed functional Mobitz II and complete heart block (*Table 3*) lend additional support for Sedmera *et al.*'s postulate and for the utility of the adult zebrafish heart model in arrhythmia studies.

4.5 Study limitations

Our study has three limitations. First, unlike the standard 12-lead ECG for humans, the standard ECG for adult zebrafish is typically obtained using only the single-lead rII.[27] To compensate for this single-lead limitation, we obtained in some zebrafish additional ECGs from leads II (*Figure 7*), rIII (*Figure 1*), and rI (*Figure 1*), one lead at a time.

Second, little is known about the complete range of pathophysiologic H_2O_2 concentrations relevant to adult zebrafish hearts. However, for H_2O_2 signalling following myocardial injury to be effective, H_2O_2 concentration at the injury site must increase suddenly and rapidly above the threshold determined by the type and severity of injury.[23] In 1- to 2-year-old zebrafish, after 20% ventricular resection, which caused no ischaemia and only a small scar, the ventricular epicardium close to the injury site produced ~30 μM of highly localized H_2O_2.[25] In contrast, ventricular cryoinjury, a superior model of mammalian myocardial infarction, likely elicits higher epicardial H_2O_2 production in response to the severe ischaemia-induced cell death and extensive ablative scar formation.[53] Experimentally, the exogenous H_2O_2 concentration of 100 μM used in the *ex vivo* experiments of this study was well within the low end of the concentration range in the literature. *Ex vivo* adult zebrafish hearts were reportedly treated with as high as 200 μM H_2O_2;[25] *in vivo* zebrafish embryos with as high as 5 mM[54,55] or 20 mM H_2O_2.[21,56]

Finally, even with state-of-the-art equipment, transmural optical mapping was limited by the spongy and trabeculated nature of the zebrafish myocardium. The thin, spongy, tapering ventricular trabeculae did not readily lend themselves to visualization in their entirety, except at their short (≤100 μm) the proximal end of compact myocardium that abuts the epicardium (Supplementary material online *Figure S9A*). This ultrashort transmural distance may explain why H_2O_2 did not reverse the transmural electrical gradient. In contrast, H_2O_2 reversal of the epicardial gradient that spread over a 15-fold longer distance of 1.5 mm could be readily captured. Nonetheless, we found that the zebrafish baseline transmural gradients of ventricular activation and repolarization are similar in polarity to the human counterparts and, therefore, could not possibly account for the zebrafish ventricular ECG patterns, which are mirror images of those in humans (*Figure 7A*). In contrast, the zebrafish epicardial electrical gradients fully accounted for its ventricular ECG patterns. Interestingly, only the zebrafish epicardium, but not the trabeculated myocardium, is required for cardiac repair and regeneration and has therefore recently become a therapeutic target in studies of cardiac repair strategies.[42] If activated by injury, the epicardium provides for cardiac regeneration a crucial source of multipotent cells and paracrine factors, including the 'necessary evil'[23] H_2O_2.[57]

4.6 Future studies

Identifying the CaMKII targets responsible for H_2O_2 reversal of the ventricular electrical gradients is the next logical pursuit because those ionic currents are also most likely responsible for establishing the ventricular electrical gradients at baseline. Additionally, while our study demonstrated the value of the healthy adult zebrafish heart model in studies of H_2O_2-induced arrhythmogenesis, we are also investigating whether a fibrotic zebrafish heart model will exhibit the same synergy between stress and fibrosis as a mechanism of arrhythmogenesis that we described for the mammalian heart.

Data availability

The group data and representative individual data underlying this article are available in the article and in its online supplementary material. Additional individual data will be shared on reasonable request to the corresponding author.

Supplementary material

Supplementary material is available at *Cardiovascular Research* online.

Acknowledgements

We thank Brady Okura from SciMedia, Kenji Tsubokura, and Toshiki Sakuraba from Brainvision for optical mapping camera and software support; Charles James from Ground Zero Graphic Communications for medical art illustration; and Dr James Weiss for critical reading of the manuscript.

Conflict of interest: none declared.

Funding

This work was supported by the National Institutes of Health (R01HL141452 to T.P.N.).

References

1. Arnaout R, Ferrer T, Huisken J, Spitzer K, Stainier DY, Tristani-Firouzi M, Chi NC. Zebrafish model for human long QT syndrome. *Proc Natl Acad Sci USA* 2007;**104**:11316–11321.
2. Nemtsas P, Wettwer E, Christ T, Weidinger G, Ravens U. Adult zebrafish heart as a model for human heart? An electrophysiological study. *J Mol Cell Cardiol* 2010;**48**:161–171.
3. Vornanen M, Hassinen M. Zebrafish heart as a model for human cardiac electrophysiology. *Channels (Austin, TX)* 2016;**10**:101–110.
4. Leong IU, Skinner JR, Shelling AN, Love DR. Zebrafish as a model for long QT syndrome: the evidence and the means of manipulating zebrafish gene expression. *Acta Physiol (Oxf)* 2010;**199**:257–276.
5. Kithcart A, MacRae CA. Using zebrafish for high-throughput screening of novel cardiovascular drugs. *JACC Basic Transl Sci* 2017;**2**:1–12.
6. Zhao Y, Zhang K, Sips P, MacRae CA. Screening drugs for myocardial disease in vivo with zebrafish: an expert update. *Expert Opin Drug Discov* 2019;**14**:343–353.
7. Milan DJ, Jones IL, Ellinor PT, MacRae CA. In vivo recording of adult zebrafish electrocardiogram and assessment of drug-induced QT prolongation. *Am J Physiol Heart Circ Physiol* 2006;**291**:H269–273.
8. Liu CC, Li L, Lam YW, Siu CW, Cheng SH. Improvement of surface ECG recording in adult zebrafish reveals that the value of this model exceeds our expectation. *Sci Rep* 2016;**6**:25073.
9. Szentadrassy N, Banyasz T, Biro T, Szabo G, Toth BI, Magyar J, Lazar J, Varro A, Kovacs L, Nanasi PP. Apico-basal inhomogeneity in distribution of ion channels in canine and human ventricular myocardium. *Cardiovasc Res* 2005;**65**:851–860.
10. Alday A, Alonso H, Gallego M, Urrutia J, Letamendia A, Callol C, Casis O. Ionic channels underlying the ventricular action potential in zebrafish embryo. *Pharmacol Res* 2014;**84**:26–31.
11. Abramochkin D V, Hassinen M, Vornanen M. Transcripts of Kv7.1 and MinK channels and slow delayed rectifier K+ current (IKs) are expressed in zebrafish (Danio rerio) heart. Pflugers Arch- Eur J Physiol 2018;**470**:1753–1764.
12. Katz AM, Katz PB. Homogeneity out of heterogeneity. *Circulation* 1989;**79**:712–717.
13. Akar FG, Rosenbaum DS. Transmural electrophysiological heterogeneities underlying arrhythmogenesis in heart failure. *Circ Res* 2003;**93**:638–645.
14. Chauhan VS, Downar E, Nanthakumar K, Parker JD, Ross HJ, Chan W, Picton P. Increased ventricular repolarization heterogeneity in patients with ventricular arrhythmia vulnerability and cardiomyopathy: a human in vivo study. *Am J Physiol Heart Circ Physiol* 2006;**290**:H79–86.
15. Glukhov AV, Fedorov VV, Lou Q, Ravikumar VK, Kalish PW, Schuessler RB, Moazami N, Efimov IR. Transmural dispersion of repolarization in failing and nonfailing human ventricle. *Circ Res* 2010;**106**:981–991.
16. Clayton RH, Holden AV. Dispersion of cardiac action potential duration and the initiation of re-entry: a computational study. *Biomed Eng Online* 2005;**4**:11.
17. Nguyen TP, Sovari AA, Pezhouman A, Iyer S, Cao H, Ko CY, Bapat A, Vahdani N, Ghanim M, Fishbein MC, Karagueuzian HS. Increased susceptibility of spontaneously hypertensive rats to ventricular tachyarrhythmias in early hypertension. *J Physiol* 2016;**594**:1689–1707.
18. Nguyen TP, Xie Y, Garfinkel A, Qu Z, Weiss JN. Arrhythmogenic consequences of myofibroblast-myocyte coupling. *Cardiovasc Res* 2012;**93**:242–251.
19. Sato D, Xie LH, Nguyen TP, Weiss JN, Qu Z. Irregularly appearing early afterdepolarizations in cardiac myocytes: random fluctuations or dynamical chaos? *Biophys J* 2010;**99**:765–773.
20. Nguyen TP, Singh N, Xie Y, Qu Z, Weiss JN. Repolarization reserve evolves dynamically during the cardiac action potential: effects of transient outward currents on early afterdepolarizations. *Circ Arrhythm Electrophysiol* 2015;**8**:694–702.
21. Inoue T, Ide T, Yamato M, Yoshida M, Tsutsumi T, Andou M, Utsumi H, Tsutsui H, Sunagawa K. Time-dependent changes of myocardial and systemic oxidative stress are dissociated after myocardial infarction. *Free Radic Res* 2009;**43**:37–46.
22. Yoo SK, Freisinger CM, LeBert DC, Huttenlocher A. Early redox, Src family kinase, and calcium signaling integrate wound responses and tissue regeneration in zebrafish. *J Cell Biol* 2012;**199**:225–234.
23. Rhee SG. Cell signaling. H_2O_2, a necessary evil for cell signaling. *Science* 2006;**312**:1882–1883.
24. Lisse TS, King BL, Rieger S. Comparative transcriptomic profiling of hydrogen peroxide signaling networks in zebrafish and human keratinocytes: implications toward conservation, migration and wound healing. *Sci Rep* 2016;**6**:20328.
25. Han P, Zhou XH, Chang N, Xiao CL, Yan S, Ren H, Yang XZ, Zhang ML, Wu Q, Tang B, Diao JP, Zhu X, Zhang C, Li CY, Cheng H, Xiong JW. Hydrogen peroxide primes heart regeneration with a derepression mechanism. *Cell Res* 2014;**24**:1091–1107.
26. McFarland WN, Klontz GW. Anesthesia in fishes. *Fed Proc* 1969;**28**:1535–1540.
27. Zhao Y, Tran M, Yun M, Nguyen SA, Nguyen TP. In vivo surface electrocardiography for adult zebrafish. J Vis Exp 2019;**150**:e60011
28. Mersereau EJ, Poitra SL, Espinoza A, Crossley DA 2nd, Darland T. The effects of cocaine on heart rate and electrocardiogram in zebrafish (*Danio rerio*). *Compar Biochem Physiol C* 2015;**172-173**:1–6.
29. Manly BFJ. Randomization, bootstrap, and Monte Carlo methods in biology. In: Carlin BP, Chatfield C, Tanner M, Zidek J, eds. *Texts in Statistical Science*. 3rd ed. Boca Raton, FL: Chapman & Hall/ CRC; 2007. p455.
30. Whitley E, Ball J. Statistics review 6: nonparametric methods. *Crit Care* 2002;**6**:509–513.
31. Hiss RG, Lamb LE, Allen MF. Electrocardiographic findings in 67,375 asymptomatic subjects. X. Normal values. *Am J Cardiol* 1960;**6**:200–231.
32. Franz MR, Bargheer K, Rafflenbeul W, Haverich A, Lichtlen PR. Monophasic action potential mapping in human subjects with normal electrocardiograms: direct evidence for the genesis of the T wave. *Circulation* 1987;**75**:379–386.
33. Arteyeva NV, Azarov JE. The role of transmural repolarization gradient in the inversion of cardiac electric field: model study of ECG in hypothermia. *Ann Noninvasive Electrocardiol* 2017;**22**:e12360.
34. Simonson E, Blackburn HJr, Puchner TC, Eisenberg P, Ribeiro F, Meja M. Sex differences in the electrocardiogram. *Circulation* 1960;**22**:598–601.
35. Linde C, Bongiorni MG, Birgersdotter-Green U, Curtis AB, Deisenhofer I, Furokawa T, Gillis AM, Haugaa KH, Lip GYH, Van Gelder I, Malik M, Poole J, Potpara T, Savelieva I, Sarkozy A, Fauchier L, Kutyifa V, Ernst S, Gandjbakhch E, Marijon E, Casadei B, Chen Y-J, Swampillai J, Hurwitz J, Varma N, ESC Scientific Document Group. Sex differences in cardiac arrhythmia: a consensus document of the European Heart Rhythm Association, endorsed by the Heart Rhythm Society and Asia Pacific Heart Rhythm Society. *Europace* 2018;**20**:1565–1565ao.
36. Woo MA, Stevenson WG, Moser DK, Trelease RB, Harper RM. Patterns of beat-to-beat heart rate variability in advanced heart failure. *Am Heart J* 1992;**123**:704–710.
37. Brennan M, Palaniswami M, Kamen P. Poincaré plot interpretation using a physiological model of HRV based on a network of oscillators. *Am J Physiol Heart Circ Physiol* 2002;**283**:H1873–1886.
38. Woo MA, Stevenson WG, Moser DK, Middlekauff HR. Complex heart rate variability and serum norepinephrine levels in patients with advanced heart failure. *J Am Coll Cardiol* 1994;**23**:565–569.
39. Langheinrich U, Vacun G, Wagner T. Zebrafish embryos express an orthologue of HERG and are sensitive toward a range of QT-prolonging drugs inducing severe arrhythmia. *Toxicol Appl Pharmacol* 2003;**193**:370–382.
40. Zon LI, Peterson RT. In vivo drug discovery in the zebrafish. *Nat Rev Drug Discov* 2005;**4**:35–44.
41. Sedmera D, Reckova M, deAlmeida A, Sedmerova M, Biermann M, Volejnik J, Sarre A, Raddatz E, McCarthy RA, Gourdie RG, Thompson RP. Functional and morphological evidence for a ventricular conduction system in zebrafish and Xenopus hearts. *Am J Physiol Heart Circ Physiol* 2003;**284**:H1152–1160.
42. Cao J, Navis A, Cox BD, Dickson AL, Gemberling M, Karra R, Bagnat M, Poss KD. Single epicardial cell transcriptome sequencing identifies Caveolin 1 as an essential factor in zebrafish heart regeneration. *Development* 2016;**143**:232–243.
43. Xie LH, Chen F, Karagueuzian HS, Weiss JN. Oxidative-stress-induced afterdepolarizations and calmodulin kinase II signaling. *Circ Res* 2009;**104**:79–86.
44. Antzelevitch C, Fish J. Electrical heterogeneity within the ventricular wall. *Basic Res Cardiol* 2001;**96**:517–527.
45. Ward CA, Giles WR. Ionic mechanism of the effects of hydrogen peroxide in rat ventricular myocytes. *J Physiol* 1997;**500**:631–642.
46. Anderson ME, Braun AP, Wu Y, Lu T, Wu Y, Schulman H, Sung RJ. KN-93, an inhibitor of multifunctional Ca++/calmodulin-dependent protein kinase, decreases early afterdepolarizations in rabbit heart. *J Pharmacol Exp Ther* 1998;**287**:996–1006.
47. Morita N, Sovari AA, Xie Y, Fishbein MC, Mandel WJ, Garfinkel A, Lin S-F, Chen P-S, Xie L-H, Chen F, Qu Z, Weiss JN, Karagueuzian HS. Increased susceptibility of aged hearts to ventricular fibrillation during oxidative stress. *Am J Physiol Heart Circ Physiol* 2009;**297**:H1594–1605.

48. Zhao Z, Xie Y, Wen H, Xiao D, Allen C, Fefelova N, Dun W, Boyden PA, Qu Z, Xie LH. Role of the transient outward potassium current in the genesis of early afterdepolarizations in cardiac cells. *Cardiovasc Res* 2012;**95**:308–316.
49. Wagner S, Ruff HM, Weber SL, Bellmann S, Sowa T, Schulte T, Anderson ME, Grandi E, Bers DM, Backs J, Belardinelli L, Maier LS. Reactive oxygen species-activated Ca/calmodulin kinase IIdelta is required for late I(Na) augmentation leading to cellular Na and Ca overload. *Circ Res* 2011;**108**:555–565.
50. Song YH, Cho H, Ryu SY, Yoon JY, Park SH, Noh CI, Lee SH, Ho WK, L-Type Ca (2. +) channel facilitation mediated by H(2)O(2)-induced activation of CaMKII in rat ventricular myocytes. *J Mol Cell Cardiol* 2010;**48**:773–780.
51. Bapat A, Nguyen TP, Lee JH, Sovari AA, Fishbein MC, Weiss JN, Karagueuzian HS. Enhanced sensitivity of aged fibrotic hearts to angiotensin II- and hypokalemia-induced early afterdepolarization-mediated ventricular arrhythmias. *Am J Physiol Heart Circ Physiol* 2012;**302**:H2331–2340.
52. Xie Y, Sato D, Garfinkel A, Qu Z, Weiss JN. So little source, so much sink: requirements for afterdepolarizations to propagate in tissue. *Biophys J* 2010;**99**:1408–1415.
53. Gonzalez-Rosa JM, Martin V, Peralta M, Torres M, Mercader N. Extensive scar formation and regression during heart regeneration after cryoinjury in zebrafish. *Development* 2011;**138**:1663–1674.
54. Wang L, Oh JY, Kim HS, Lee W, Cui Y, Lee HG, Kim YT, Ko JY, Jeon YJ. Protective effect of polysaccharides from Celluclast-assisted extract of Hizikia fusiforme against hydrogen peroxide-induced oxidative stress in vitro in Vero cells and in vivo in zebrafish. *Int J Biol Macromol* 2018;**112**:483–489.
55. Cho SH, Heo SJ, Yang HW, Ko EY, Jung MS, Cha SH, Ahn G, Jeon YJ, Kim KN. Protective effect of 3-bromo-4,5-dihydroxybenzaldehyde from *Polysiphonia morrowii* harvey against hydrogen peroxide-induced oxidative stress in vitro and in vivo. *J Microbiol Biotechnol* 2019;**29**:1193–1203.
56. Panieri E, Millia C, Santoro MM. Real-time quantification of subcellular H_2O_2 and glutathione redox potential in living cardiovascular tissues. *Free Radic Biol Med* 2017;**109**:189–200.
57. Lepilina A, Coon AN, Kikuchi K, Holdway JE, Roberts RW, Burns CG, Poss KD. A dynamic epicardial injury response supports progenitor cell activity during zebrafish heart regeneration. *Cell* 2006;**127**:607–619.

Translational perspective

Zebrafish electrocardiograms remarkably recapitulate human electrocardiograms in health and disease. Yet, the underlying tissue mechanisms were unknown. This study provides the first demonstration that the baseline electrical gradients that shape zebrafish ventricular electrocardiograms are opposite human electrical gradients. Additionally, like mammalian hearts, zebrafish hearts are susceptible to CaMKII-mediated H_2O_2 proarrhythmic perturbations. Despite its vital role in zebrafish cardiac regeneration following injury, H_2O_2 can disrupt zebrafish sinus node activity, cause all three types of atrioventricular blocks, and reverse ventricular electrical gradients. These findings highlight the clinical relevance, utility, and limitations of the adult zebrafish heart as a model for mammalian arrhythmogenesis studies.